Subwavelength-Structured High-Efficiency Nanophotonic Coupler for Air Top-Cladded Silicon Waveguide

Yuhan Sun, Ting Li, Peiji Zhou, and Yi Zou, *Member, IEEE*

***Abstract*—Efficient coupling between an optical fiber and silicon waveguide has been a major practical challenge for silicon photonics since the first day due to the huge mode size mismatch between them. In this paper, we propose a subwavelength structured edge coupler for efficient coupling light into/out from air top-cladded silicon waveguides. Through refractive index engineering, we demonstrate a single-step patterned coupler with a coupling loss of ∼2.5 dB for the wavelength range from 1.5 μm to 1.65 μm.**

***Index Terms*—Subwavelength, edge coupler, silicon photonics.**

I. Introduction

DUE to the huge mode size mismatch between an optical fiber and an on-chip silicon waveguide, efficient coupling between them is always a big challenge for silicon photonics. Grating couplers [1]–[5] and mode size converter (MSC)-based edge couplers [6]–[18] are widely used for solving this issue. Compared with grating couplers, MSC-based edge couplers provide higher efficiency and broader bandwidth. This type of couplers usually expands the guiding mode size to match the fiber mode by gradually taper down the waveguide widths [12]–[14] or spatial splitting light into multiple closely-packed channels, namely trident structure [15],[16], biconical structure [17], and double trident structure [18]. Recently, subwavelength structures [19]–[21], which can provide an artificial equivalent refractive index by adjusting its duty cycle, have attracted a lot of interest. Subwavelength structured MSC-based edge couplers, which can circumvent the fixed value of the refractive indices of the constituent materials in integrated photonics, have been demonstrated [18], [22]–[24]. All of these structures typically require small waveguide width for expanding the mode size and an additional top layer, such as Polymer, Si_3N_4, SiON, SiO_2, etc., for preventing guiding mode leakage to the substrate during the coupling process. However, for certain applications, such as sensing applications, an edge coupler with air top cladding is desired, which challenges the current approaches.

In this paper, we propose an MSC-based edge coupler to efficiently couple light from an optical fiber to a silicon waveguide with air top cladding. Subwavelength structures are employed to form a single-step patterned edge coupler, featuring a coupling loss of ∼2.5 dB for the wavelength range from 1.5 μm to 1.65 μm.

II. Working Principle

The coupling loss of the edge coupler is mainly from two aspects: the first aspect is the loss from mode overlap between the fiber mode and the mode near the chip facet; the second one is the conversion loss from a subwavelength waveguide to a conventional strip waveguide. Therefore, in order to obtain a better coupling efficiency, we start from mode overlap, η, calculation between the fiber and waveguide modes [25]:

$$\eta = \frac{\left|\int F(y,z)\, W'(y,z)\, dydz\right|^2}{\int F(y,z)\, F'(y,z)\, dydz \int W(y,z)\, W'(y,z)\, dydz} \quad (1)$$

Here *F(y,z)* is the complex amplitude of the fiber mode and *W(y,z)* is the complex amplitude of the waveguide mode, and the ' symbol represents the complex conjugate. The output mode profile of a typical lens fiber is plotted in Fig. 1(b), showing a 3 μm diameter. Considering a standard 220 nm thick silicon waveguide with arbitrary refractive index, air top cladding, and SiO_2 bottom cladding, we employ the finite-difference eigenmode (FDE) solver from Lumerical to scan the TE mode overlap of waveguides with different widths. From the results shown in Fig. 1(a), we observe when the waveguide width is within the range of 2.3-4.8 μm and the expected refractive index in the range of 1.7-1.9, the overlap between the fiber emission mode reaches a peak, of which a maximized overlap about 59% happened when the refractive index is 1.79 and the width is 3.84 μm. The corresponding mode profile is plotted in Fig. 1(c). Therefore, we chose it as the end facet of our coupler. For comparison, we also plot mode profiles of a 2 μm wide waveguide

Manuscript received June 25, 2021; revised July 29, 2021; accepted August 9, 2021. Date of publication August 11, 2021; date of current version September 2, 2021. This work was supported in part by National Natural Science Foundation of China under Grant 61705099, in part by the Natural Science Foundation of Shanghai under Grant 21ZR1443100, and in part by Science and Technology Commission of Shanghai Municipality under Grant Y7360k1D01. *(Corresponding author: Yi Zou.)*

Yuhan Sun and Ting Li are with the School of Information Science and Technology, ShanghaiTech University, Shanghai 201210, China, and with the Shanghai Institute of Microsystem and Information Technology, Chinese Academy of Sciences, Shanghai 200050, China, and also with the University of Chinese Academy of Sciences, Beijing 100049, China (e-mail: sunyh@shanghaitech.edu.cn; liting@shanghaitech.edu.cn).

Peiji Zhou is with the School of Information Science and Technology, ShanghaiTech University, Shanghai 201210, China (e-mail: zhoupj@shanghaitech.edu.cn).

Yi Zou is with the School of Information Science and Technology, ShanghaiTech University, Shanghai 201210, China, and also with the Shanghai Engineering Research Center of Energy Efficient and Custom AI IC, Shanghai 201210, China (e-mail: zouyi@shanghaitech.edu.cn).

Digital Object Identifier 10.1109/JPHOT.2021.3104061

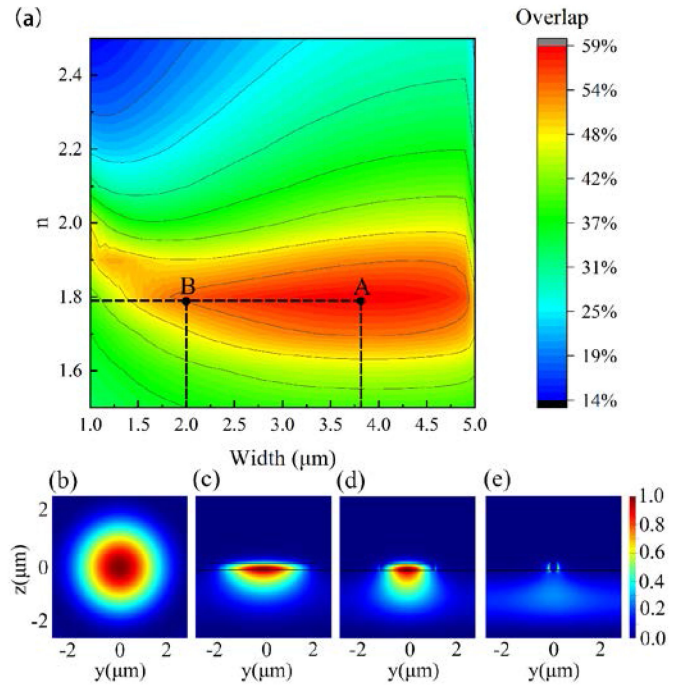

Fig. 1. (a) Calculated TE mode overlap between the fundamental lens fiber mode and a waveguide mode as a function of waveguide width, w, and material refractive index, n. Here we fix the height of waveguides to 220 nm. Simulated the fundamental optical mode of a lens fiber (b), a waveguide at Point A with $n = 1.79$, $w = 3.84$ μm (c), a waveguide at Point B with $n = 1.79$, $w = 2$ μm (d), and a silicon waveguide with $n = 3.476$, $w = 250$ nm (e).

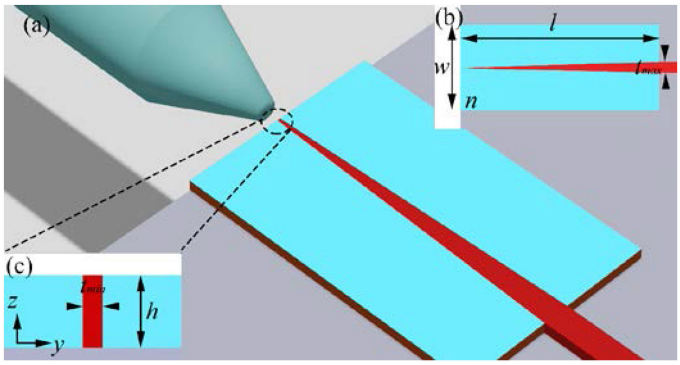

Fig. 2. (a) Schematic of the proposed coupler with an artificial lateral cladding. The red, blue, gray, and white part stands for silicon, an artificial material with the refractive index of $n = 1.79$, SiO_2, and air, respectively. The coupler width and height are fixed to 3.84 μm and 220 nm; (b) The top view of the coupler; (c) The cross-section of the coupler facet.

with $n = 1.79$ and a 250 nm wide silicon waveguide with n = 3.476 in Figs. 1(d) and (e), respectively, showing much smaller mode overlap with the typical lens fiber mode in Fig. 1(b).

The next step is to design a taper structure to efficiently convert the light into a conventional 500 nm wide silicon waveguide. The proposed coupler is shown in Fig. 2, where the red, blue, gray, and white part stands for silicon, an artificial material with the refractive index of $n = 1.79$, SiO_2, and air, respectively. We keep the surrounding material unchanged and introduce an inverse silicon taper to gradually convert the light dispersed in

TABLE I
OPTIMIZED COUPLER DESIGN WITH AN ARTIFICIAL HOMOGENEOUS MATERIAL

l	w	h	t_{min}	t_{max}	n
45μm	3.84μm	220nm	60nm	500nm	1.79

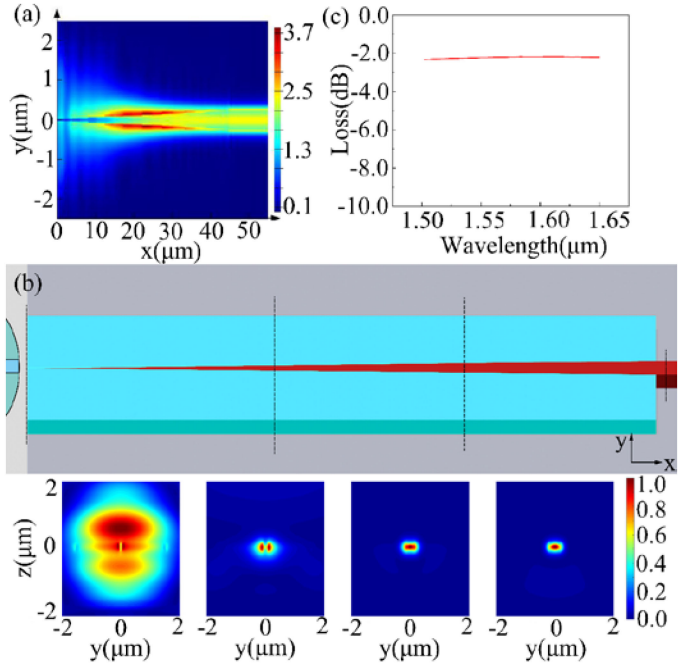

Fig. 3. Characteristics of the proposed coupler with uniform material: (a) Mode evolution; (b) The cross-section mode profiles at different positions ($x = 0$, 15, 30, 45 μm); (c) Coupling loss for wavelengths from 1.5 μm to 1.65 μm.

the outer region into the silicon waveguide. During this process, we fix the width, w, and height, h, of the coupler to 3.84 μm and 220 nm, and the minimum, t_{min}, and maximum, t_{max}, width of the inverse silicon taper to 60 nm and 500 nm, respectively, and use 3D finite difference time domain (FDTD) to scan the length, l, of the coupler. With a 3 μm diameter input Gaussian beam, we optimize the coupler design to achieve the best coupling efficiency. The optimized parameters are summarized in Table I.

Fig. 3(a) gives the mode evolution from the end facet to a conventional silicon waveguide with 500 nm in the optimized coupler. After coupling from the input lens fiber, the energy first diffuses into the artificial material and then gradually transfers to the central silicon waveguide and form a fundamental guiding mode as it propagates along the coupler. Note that there are two dark red regions along the inverse silicon taper due to the electric field discontinuity of TE mode. As the silicon waveguide becomes wider, more energy is confined at the center, reducing the electric field intensity at the boundary. The cross-section view of the mode evolution is plotted in Fig. 3(b), showing the mode conversion from the loose confined status at the facet to the well-confined mode. During the whole process, no other modes are observed which guarantees a high conversion efficiency. The coupler loss from the input fiber to the conventional silicon waveguide, shown in Fig. 3(c), is about 2.2 dB for 1.55 μm

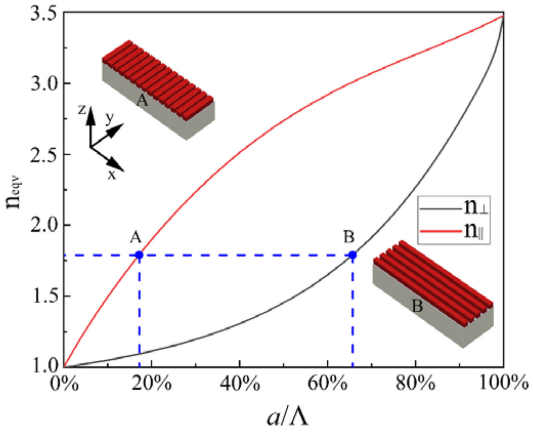

Fig. 4. The equivalent refractive index of the subwavelength periodic structured waveguide for different duty cycles, calculated by effective medium theory at second-order approximation. The red/black curve corresponds to Device A/B with a period along/ perpendicular to the propagation direction.

wavelength and almost flat for the whole wavelength region from 1.5 μm to 1.65 μm.

III. Subwavelength Structured Coupler

In reality, it is difficult to find and grow material that matches the refractive index of our design, we thus choose to replace it with subwavelength structures. The subwavelength structure consists of periodically arranged dielectric elements, and since the period of the structure is much smaller than the wavelength, the whole structure can be viewed as an equivalent homogeneous medium. By adjusting the duty cycle of the subwavelength structure, we can tune its equivalent refractive index based on effective medium theory (EMT) as [19]:

$$n_{\parallel}^2 \approx \frac{a}{\Lambda} n_1^2 + \left(1 - \frac{a}{\Lambda}\right) n_2^2 + \mathrm{O}\left(\frac{\Lambda^2}{\lambda^2}\right) \tag{2}$$

$$n_{\perp}^{-2} \approx \frac{a}{\Lambda} n_1^{-2} + \left(1 - \frac{a}{\Lambda}\right) n_2^{-2} + \mathrm{O}\left(\frac{\Lambda^2}{\lambda^2}\right) \tag{3}$$

Here, $n_{\parallel}$ and $n_{\perp}$ correspond to the electric field parallel and perpendicular to the subwavelength periodic interfaces, respectively. Λ is the period of the structure, a is the width of the material with refractive index n_1, and $\frac{a}{\Lambda}$ stands for the duty cycle. The curves of these two equations are plotted in Fig. 4.

We first try to design a one-dimensional subwavelength structure that can function as the artificial material with $n = 1.79$. There are two approaches to achieve this target, namely building subwavelength period along or perpendicular to the propagation direction, x, shown in Fig. 4. In both these two cases, we set $n_1 = 3.476$ and $n_2 = 1$. For the period along the propagation direction, according to Eqn. 2 with a second-order approximation, we can draw the red curve in Fig. 4. From this curve, we can get an equivalent refractive index of 1.79 when the duty cycle is 17%, corresponding to a silicon strip array, Device A in Fig. 4, with a 300 nm period and each strip is 51 nm wide in the x-direction, 3.84 μm long in the y-direction. For the period perpendicular to the propagation direction, we use Eqn. 3 with a second-order approximation to plot the black curve in Fig. 4, and get a 300 nm pitched silicon strip array, Device B in Fig. 4, with each strip 198 nm wide in the y-direction, corresponding to a duty cycle of 66%. Assuming the taper is 45 μm long in the x-direction for better mode transition, both these methods result in slender silicon strips with an aspect ratio, which is the ratio between the long side and the short side, larger than 70, which sets a big challenge for device fabrication.

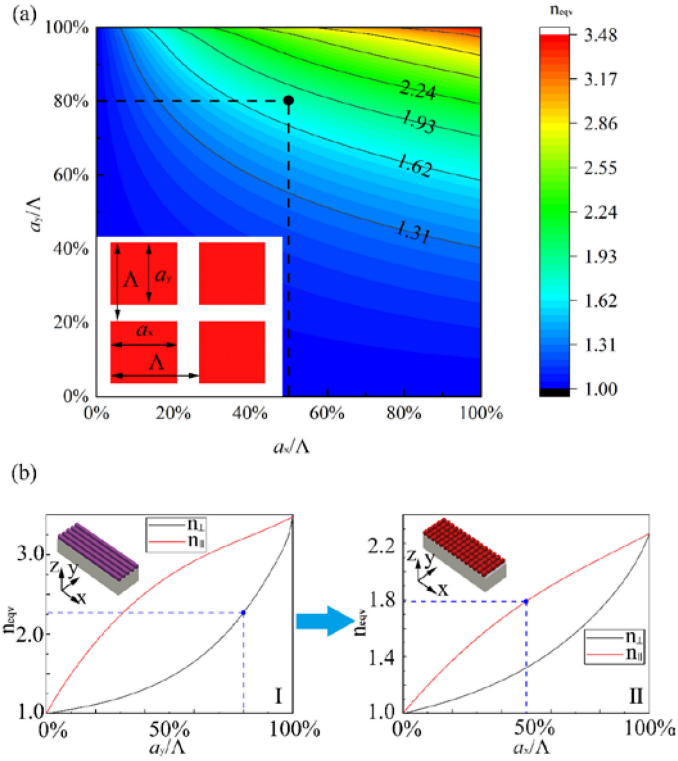

Fig. 5. (a) The equivalent refractive index of the two-dimensional subwavelength periodic structured waveguide as a function of duty cycles along and perpendicular to the propagation direction, calculated by effective medium theory at second-order approximation. The black point represents the equivalent refractive index of 1.79. (b) The process to achieve the equivalent refractive index of the two-dimensional subwavelength periodic structured waveguide.

Since matching the optimized facet waveguide by a one-dimensional subwavelength periodic structure would require multiple slender silicon strips and would be too demanding for processing, we chose a two-dimensional subwavelength structure. By introducing the subwavelength structure in both the parallel and perpendicular directions, we can obtain a desired refractive index, while releasing the complexity of the fabrication process. Setting 300 nm as the periods for both the x-direction and y-direction for simplicity, we can obtain the target equivalent refractive index of 1.79 when the duty cycles of x-direction and y-direction are 0.5, and 0.8, respectively as shown in Fig. 5(a). To achieve this result, as shown in Fig. 5(b), we do a two-step EMT calculation. The first is to calculate the structure with the period perpendicular to the propagation direction, x, namely duty cycle in the y-direction, $\frac{a_y}{\Lambda}$, as shown in the left figure of Fig. 5(b). Considering a minimum feature size of 60 nm we can build, a duty cycle of 80% corresponding

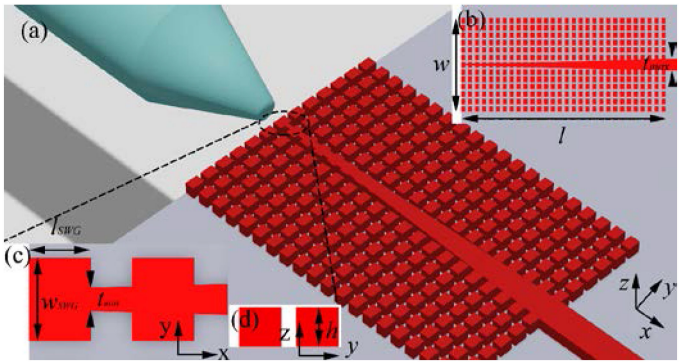

Fig. 6. (a) Schematic of the proposed two-dimensional subwavelength structured coupler; (b) The top view of the coupler; (c) The zoom-in image of the top view; (d) The cross-section of the coupler facet.

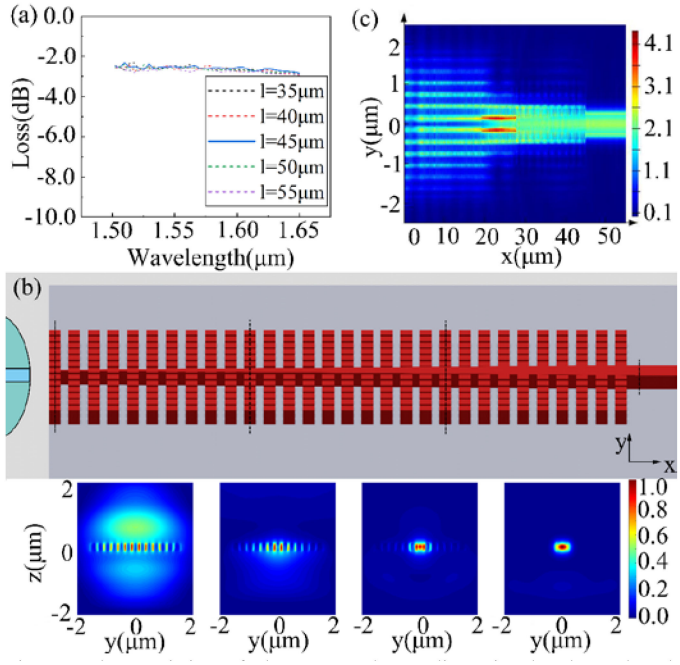

Fig. 7. Characteristics of the proposed two-dimensional subwavelength structured coupler: (a) Coupling loss of couplers with different lengths for wavelengths from 1.5 μm to 1.65 μm; (b) The cross-section mode profiles at different positions ($x = 0$, 15, 30, 45 μm); (c) Mode evolution.

to an equivalent refractive index of 2.268 is chosen. After that we fix the high index material as 2.268 and the low index as 1, we choose the duty cycle along the propagation direction, $\frac{a_x}{\Lambda}$, as 50% to achieve an equivalent index of 1.79 which provides the best overlap as mentioned in the previous section. Note that, since we only consider the TE polarized light, for Step-I, the period perpendicular to the propagation direction, the black curve represents the structure-property; for Step-II, the period along the propagation direction, the red curve describes the structure-property. By combining these two, a two-dimensional subwavelength structured silicon waveguide array with a length of 150 nm along the x-direction and a width of 60 nm along the y-direction is formed to equivalently replace a uniform medium with a refractive index of 1.79.

For a better transition from the subwavelength coupler to a strip waveguide of 500 nm wide, we choose to linearly taper up the silicon waveguide from 60 nm, the limitation of our fabrication process, to 500 nm and laterally clad it with the subwavelength structure, shown in Fig. 6. The length, width, and height of the subwavelength structure elements are taken from the previous section, namely $l_{SWG} = 150$ nm, $w_{SWG} = 240$ nm, and $h = 220$ nm. Also, the width, w, of the taper and the period of the subwavelength structure along and perpendicular to the propagation directions, Λ, are kept to 3.84 μm and 300 nm, respectively. We then perform the length scanning to minimize the mode conversion loss at 1.55 μm.

The subwavelength structured couplers with different lengths, Fig. 7(a), are simulated with the same Gaussian light source as mentioned in the previous section, and we monitor the mode profile along the propagation direction every 15 μm, Figs. 7(b) and (c). Comparing with other lengths, the 45 μm long taper provides a more stable coupling loss and relatively larger bandwidth. The optimized parameters are summarized in Table II, and the characteristics are plotted in Fig. 7. Similar to the artificial homogeneous-material-based coupler, the input light diffuses in the subwavelength structure at first, and gradually converges to the central silicon taper to form a guiding mode in a 500 nm conventional waveguide. The cross-section evolution is shown in Fig. 7(b). Unlike the homogeneous one, at the facet, the light is more at the central subwavelength structure, showing several high-intensity spots. As the taper becomes wider, light is more concentrated into the center and forms a fundamental waveguide mode. The coupling loss of less than 2.5 dB is observed for the wavelengths from 1.5 μm to 1.65 μm. The results match with the homogeneous coupler reasonably well with a slightly higher coupling loss due to the approximation of the EMT. Further push the period of the subwavelength structure towards the deep subwavelength region, could solve this issue and lead to a better fit to the theoretical prediction.

TABLE II
OPTIMIZED COUPLER DESIGN WITH TWO-DIMENSIONAL SUBWAVELENGTH STRUCTURE

l_{SWG}	w_{SWG}	h	t_{min}	t_{max}	Λ	w	l
150nm	240nm	220nm	60nm	500nm	300nm	3.84μm	45μm

For practical application, it is difficult to control the facet position with 100 nm accuracy, which means the facet may locate at different positions within one subwavelength period. To figure out the impact of such deviation, we also carry out the simulations of the cutting plane positions and plot them in Fig. 8. We pick four positions for the cutting plane, as marked A, B, C, and D in the inset of Fig. 8. Position B provides the best performance. Slight lower efficiency happens for the other three locations. However, all the four couplers have similar coupling loss and bandwidth, namely, the tip position is not very critical for this type of coupler, which greatly releases the difficulty of measurement.

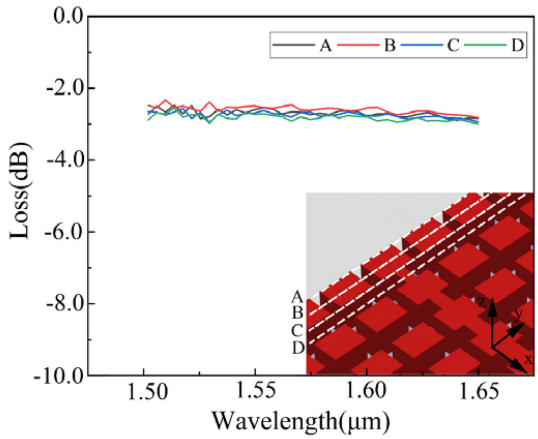

Fig. 8. Coupling loss of two-dimensional subwavelength structured coupler with different facet locations. The inset shows the locations of four cutting planes.

IV. Conclusion

We propose a high-efficiency edge coupler for silicon waveguides with air top cladding. The coupler has a coupling loss of 2.5 dB in the wavelength range 1.5 μm – 1.65 μm. A two-dimensional subwavelength structure is employed to effectively reduces the refractive index of the silicon waveguide and better match the mode field of a lens fiber. To the best of our knowledge, this is the first edge coupler for silicon waveguides with air top cladding. Our approach will be easily applied to other material systems, such as silicon-on-sapphire, germanium-on-silicon, *et al.* It would be extremely important for mid-infrared applications, where the commonly used materials become lossy in this regime.

References

[1] C. Alonso-Ramos, P. Cheben, A. Ortega-Moñux, J. Schmid, D.-X. Xu, and I. Molina-Fernández, "Fiber-chip grating coupler based on interleaved trenches with directionality exceeding 95%," *Opt. Lett.*, vol. 39, no. 18, pp. 5351–5354, 2014.

[2] D. Benedikovic *et al.*, "High-efficiency single etch step apodized surface grating coupler using subwavelength structure," *Laser Photon. Rev.*, vol. 8, no. 6, pp. L93–L97, 2014.

[3] Y. Zou, *et al.*, "Grating-coupled silicon-on-sapphire integrated slot waveguides operating at mid-infrared wavelengths," *Opt. Lett.*, vol. 39, no. 10, pp. 3070–3073, 2014.

[4] D. Benedikovic *et al.*, "L-shaped fiber-chip grating couplers with high directionality and low reflectivity fabricated with deep-UV lithography," *Opt. Lett.*, vol. 42, no. 17, pp. 3439–3442, 2017.

[5] Y. Wang *et al.*, "Design of broadband subwavelength grating couplers with low back reflection," *Opt. Lett.*, vol. 40, no. 20, pp. 4647–4650, 2015.

[6] G. Roelkens, P. Dumon, W. Bogaerts, D. Van Thourhout, and R. Baets, "Efficient silicon-on-insulator fiber coupler fabricated using 248-nm-deep UV lithography," *IEEE Photon. Technol. Lett.*, vol. 17, no. 12, pp. 2613–2615, Dec. 2005.

[7] S. J. McNab, N. Moll, and Y. A. Vlasov, "Ultra-low loss photonic integrated circuit with membrane-type photonic crystal waveguides," *Opt. Exp.*, vol. 11, no. 22, pp. 2927–2939, 2003.

[8] T. Tsuchizawa *et al.*, "Microphotonics devices based on silicon microfabrication technology," *IEEE J. Sel. Top. Quantum Electron.*, vol. 11, no. 1, pp. 232–240, Jan./Feb. 2005.

[9] B. B. Bakir *et al.*, "Low-loss ($<$ 1 dB) and polarization-insensitive edge fiber couplers fabricated on 200-mm silicon-on-insulator wafers," *IEEE Photon. Technol. Lett.*, vol. 22, no. 11, pp. 739–741, Jun. 2010.

[10] K. Kasaya, O. Mitomi, M. Naganuma, Y. Kondo, and Y. Noguchi, "A simple laterally tapered waveguide for low-loss coupling to single-mode fibers," *IEEE Photon. Technol. Lett.*, vol. 5, no. 3, pp. 345–347, Mar. 1993.

[11] N. Hatori *et al.*, "A hybrid integrated light source on a silicon platform using a trident spot-size converter," *J. Lightw. Technol.*, vol. 32, no. 7, pp. 1329–1336, 2014.

[12] V. R. Almeida, R. R. Panepucci, and M. Lipson, "Nanotaper for compact mode conversion," *Opt. Lett.*, vol. 28, no. 15, pp. 1302–1304, 2003.

[13] L. Vivien, S. Laval, E. Cassan, X. L.. Roux, and D. Pascal, "2-D taper for low-loss coupling between polarization-insensitive microwaveguides and single-mode optical fibers," *J. Lightw. Technol.*, vol. 21, no. 10, pp. 2429, 2003.

[14] A. Sure, T. Dillon, J. Murakowski, C. Lin, D. Pustai, and D. W. Prather, "Fabrication and characterization of three-dimensional silicon tapers," *Opt. Exp.*, vol. 11, no. 26, pp. 3555–3561, 2003.

[15] N. Hatori, *et al.*, "A hybrid integrated light source on a silicon platform using a trident spot-size converter," *J. Lightw. Technol.*, vol. 32, no. 7, pp. 1329–1336, 2014.

[16] Y. Urino *et al.*, "High-density and wide-bandwidth optical interconnects with silicon optical interposers," *Photon. Res.*, vol. 2, no. 3, pp. A1–A7, 2014.

[17] S. H. Tao, J. Song, Q. Fang, M. B. Yu, G. Q. Lo, and D. L. Kwong, "Improving coupling efficiency of fiber-waveguide coupling with a double-tip coupler," *Opt. Exp.*, vol.vol. 16, no. 25, pp. 20803–20808, 2008.

[18] A. He, X. Guo, K. Wang, Y. Zhang, and Y. Su, "Low loss, large bandwidth fiber-chip edge couplers based on silicon-on-insulator platform," *J. Lightw. Technol.*, vol. 38, no. 17, pp. 4780–4786, 2020.

[19] P. Cheben, R. Halir, J. H. Schmid, H. A. Atwater, and D. R. Smith, "Subwavelength integrated photonics," *Nature*, vol. 560, no. 7720, pp. 565–572, 2018.

[20] R. Halir *et al.*, "Waveguide sub-wavelength structures: A review of principles and applications," *Laser Photon. Rev.*, vol. 9, no. 1, pp. 25–49, 2015.

[21] R. Halir *et al.*, "Subwavelength-grating metamaterial structures for silicon photonic devices," *Proc. IEEE*, vol. 106, no. 12, pp. 2144–2157, Dec. 2018.

[22] P. Cheben, D. Xu, S. Janz, and A. Densmore, "Subwavelength waveguide grating for mode conversion and light coupling in integrated optics," *Opt. Exp.*, vol. 14, no. 11, pp. 4695–4702, 2006.

[23] P. Cheben *et al.*, "Refractive index engineering with subwavelength gratings for efficient microphotonic couplers and planar waveguide multiplexers," *Opt. Lett.*, vol. 35, no. 15, pp. 2526–2528, 2010.

[24] T. Barwicz *et al.*, "Integrated metamaterial interfaces for self-aligned fiber-to-chip coupling in volume manufacturing," *IEEE J. Sel. Topics Quantum Electron.*, vol. 25, no. 3, pp. 1–13, May/Jun. 2018.

[25] Z. Pan *et al.*, "Quasi-vertical tapers for polymer-waveguide-based interboard optical interconnects," *Photon. Res.*, vol. 3, no. 6, pp. 317–323, 2015.